Journal of the Korean Nuclear Society
Volume 30, Number 3, pp.245~261, June 1998

A Study on Validation of Variable Aperture Channel Model: Migration Experiments of Conservative Tracer in Parallel and Wedge-Shaped Fracture

D.K. Keum and P.S. Hahn
Korea Atomic Energy Research Institute
150 Dukjin-dong, Yusung-gu, Taejon 305-353, Korea

T.T. Vandergraaf
Whiteshell Laboratories
Pinawa, Manitoba, Canada ROE 1LO

(Received November 11, 1997)

Abstract

In order to validate the variable aperture channel model that can deal with the non-uniform flow rate in flow domain, migration experiments of conservative tracer were performed in two artificial fractures, a parallel and a wedge-shaped fracture. These different fracture shapes were designed to give different flow pattern. The fractures were made from a transparent acrylic plastic plate and a granite slab with dimensions of 10 × 61 × 61 cm. Uranine (Fluorescein sodium salt) was used as a conservative tracer. The volumetric flow rates of uranine feed solution were 30 mL/ hr, giving a mean residence time in the fracture of approximately 24 hours for the parallel fracture and 34 hours for the wedge-shaped fracture. The migration plumes of uranine were photographed to obtain profiles in space and time for movement of a tracer in fractures. The photographed migration plume was greatly affected by the geometric shape of fractures. The variable aperture channel model could have predicted the experimental results for the parallel fracture with a large accuracy. It is expected that the variable aperture channel model would be effective to predict the transport of the contaminant, especially, with the flow rate variation in a fracture.

1. Introduction

Modeling for migration of contaminants in fractured rock and its validation have been an important subject for safety assessment of nuclear waste disposal. A number of migration models have been developed to deal with complex hydrological and physicochemical phenomena in fractured rock. In many cases a fracture has been modeled as a pair plates with a constant aperture width, giving a uniform flow rate across the fracture [1-5]. However, the shape of natural fractures is too various to be uniform and data obtained from field

experiments showed the heterogeneous flow behavior of groundwater in fractured rock [6-8]. Therefore, representing a fracture by a pair of parallel plates with a constant aperture width may be inadequate to describe actual fluid movement in a fracture. To consider the variation of aperture width in a fracture, Neretnieks et al. [9] and Keum et al. [10] developed a stratified channel model in which flow takes place through hypothetically independent channels, each with a constant aperture width and with a distribution of aperture values. Tsang and his coworkers [11-12] and Moreno et al. [13] developed the variable aperture channel model in which the water flow rate between channels varies due to different aperture width and causes channeling dispersion. Between the aforementioned two models, the variable aperture channel model seems to be more appropriate to deal with complex flow pattern in fractured rock because it can consider the flow across each channel. The variable aperture channel model could be more practical in the safety assessment of nuclear waste disposal when effects of sorption and rock matrix diffusion are considered in the model. Even though some studies have described the possibility to incorporate sorption and rock matrix diffusion in the variable aperture channel model, to our knowledge, none of studies has attempted to consider both effects simultaneously, especially rock matrix diffusion in the model. In this work, the variable aperture channel model in which sorption and rock matrix diffusion are considered is derived with sound mathematical basis.

In parallel with model development, many experimental attempts have been made to validate contaminant transport models. Among them, only a few cases have been focused on the validation of the variable aperture channel model. Kimura and Munakata [14] analyzed experimental breakthrough curves that were the test case 2 of International INTRAVAL project under auspices of OECD/NEA using the variable aperture channel model. In their study, the fracture was considered as a black box because the aperture width distribution was unknown. Strictly speaking, the migration experiment with unknown aperture width distribution is not appropriate to validate the variable aperture channel model because we could not estimate quantitatively how much well the model predict the actual flow in a fracture. Park et al. [15] performed the migration experiment of tracer in a natural granite fracture. However, they also could not have measured the flow profile in the fracture so that the actual flow pattern in space and time in the fracture was not validated. In this point of view, the experiment to obtain migration plume of a tracer in space and time in a fracture appears to be a critical method to validate the variable aperture channel model.

This study has been performed with two purposes. One is to derive the variable aperture channel model in which sorption and rock matrix diffusion are considered with sound mathematical basis and the other is to validate the model by a new migration experimental approach. For the migration experiment for validation, two different fracture shapes, a fracture with a rectangular cross section and a wedge-shaped fracture with the wedge dipping across the flow field, were designed to investigate whether the model could well predict flow pattern depending on fracture shapes. Uranine (Fluorescein sodium salt) dye was used as conservative tracer and the migration profile of the dye in the fracture was photographed at 3 hours intervals. This experimental method provides migration data of a tracer in time and space in fracture and allows the comparison of

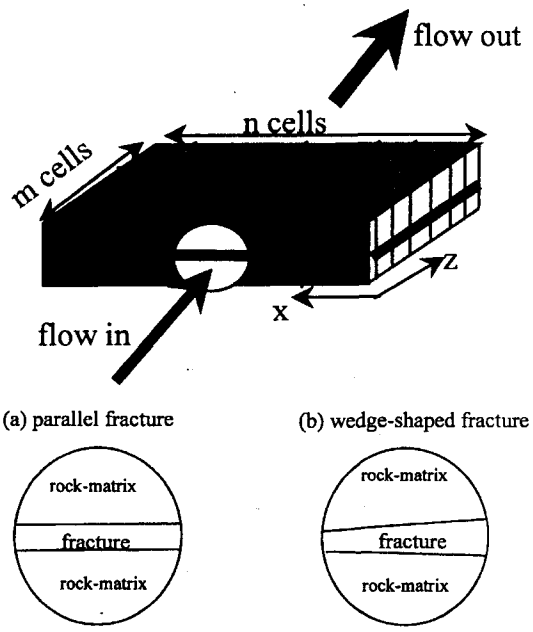

Fig. 1. Conceptual Diagram for Modeling of (a) the Parallel and (b) the Wedge-Shaped Fracture.

the predicted with the experimental migration plume directly.

2. Variable Aperture Channel Model

2.1. Flow Model

The aperture width of most natural fractures varies along the flow path, forming unevenly distributed flow along the fracture plane. To model the variation of aperture width, a fracture can be modeled as a group of cells with different aperture width as shown in Fig.1. The fracture is divided into n cells in the transverse direction and m cells in the longitudinal direction (flow direction), to give total $n \times m$ cells. The aperture width of each cell is assumed to be constant.

The steady state flow rate of an incompressible fluid through the fracture with constant aperture width ($\overline{b}$) can be expressed by the cubic law:

$$Q = \frac{\rho g \overline{b}^3}{12\mu} L_x \Delta h / L_z \tag{1}$$

where Q (ml/sec) is the net flow rate through the fracture, ρ (g/ml) is the density of water, g(cm/sec^2) is the acceleration due to gravity, μ (g/cm.sec) is the dynamic viscosity of water, L_z is the fracture length, L_x is the fracture width and Δh(cm) is the pressure head difference of flow between inlet and outlet of the fracture. Eq.(1) can be applied to each of cells in Fig.1 because the aperture width of each cell has been assumed to be constant. When aperture widths of two adjacent cells i and j, are given by $\overline{b_i}$ and $\overline{b_j}$, respectively, width and length of each cell are given by $\Delta x(=L_x / n)$ and $\Delta z(=L_z / m)$, respectively and the volumetric fluid flow rate from cell i to adjacent cell j is given by $q_{i,j}$, then the pressure head difference of the flow between cell i and j can be expressed by [13]:

$$\Delta h_{ij} = \frac{q_{i,j}}{\frac{\rho g \overline{b_i}^3}{12\mu}\Delta x \frac{2}{\Delta z}} + \frac{q_{i,j}}{\frac{\rho g \overline{b_j}^3}{12\mu}\Delta x \frac{2}{\Delta z}}$$
$$= q_{i,j}\left[\frac{6\mu}{\rho g}\frac{\Delta x}{\Delta z}\left(\frac{1}{\overline{b_i}^3} + \frac{1}{\overline{b_j}^3}\right)\right] = q_{i,j} R_{i,j} \tag{2}$$

where $R_{i,j}$ is called as the flow resistance between cells i and j. Because there is no water accumulation in a fracture under steady state conditions, the mass balance around the cell i can be expressed as (Fig.2):

$$q_{i,1} + q_{i,2} + q_{i,3} + q_{i,4} = 0 \tag{3}$$

It is noted that there are four neighbors around cell i in a two-dimensional flow model. Substituting the relationship of Eq.(2) into Eq.(3), we obtain a set of linear algebra equations given by

$$\frac{h_i - h_{i-n}}{R_{i,1}} + \frac{h_i - h_{i+1}}{R_{i,2}} + \frac{h_i - h_{i+n}}{R_{i,3}} + \frac{h_i - h_{i-1}}{R_{i,4}} = 0 \tag{4}$$

(i = 1, 2, 3, ·····, nm)

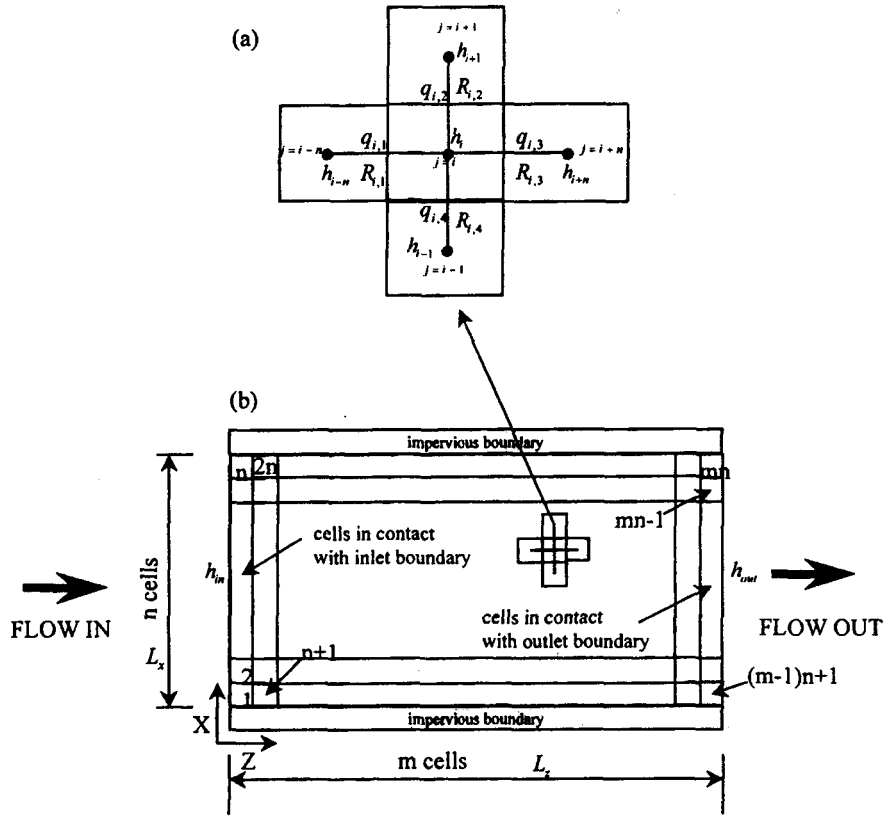

Fig. 2(a) Flow Around Cell *i* and its Four Surrounding Neighbors
(b) Two-Dimensional Rectangular Grid Used in the Modeling.

where

$$R_{i,1} = \frac{6\mu}{\rho g}\frac{\Delta z}{\Delta x}\left(\frac{1}{\bar{b}_i^3} + \frac{1}{\bar{b}_{i-n}^3}\right) \quad (5)$$

$$R_{i,2} = \frac{6\mu}{\rho g}\frac{\Delta x}{\Delta z}\left(\frac{1}{\bar{b}_i^3} + \frac{1}{\bar{b}_{i+1}^3}\right) \quad (6)$$

$$R_{i,3} = \frac{6\mu}{\rho g}\frac{\Delta z}{\Delta x}\left(\frac{1}{\bar{b}_i^3} + \frac{1}{\bar{b}_{i+n}^3}\right) \quad (7)$$

$$R_{i,4} = \frac{6\mu}{\rho g}\frac{\Delta x}{\Delta z}\left(\frac{1}{\bar{b}_i^3} + \frac{1}{\bar{b}_{i-1}^3}\right) \quad (8)$$

Boundary conditions were assumed as

$$h_{i-n} = h_{in},\ i = 1,2,\cdots,n \quad (9)$$

$$h_{i+n} = h_{out},\ i = n(m-1)+1,\ n(m-1)+2,\ \cdots,\ mn \quad (10)$$

$$q_{i,2} = 0,\ i = n, 2n, 3n, \cdots, nm \quad (11)$$

$$q_{i,4} = 0,\ i = 1, n+1, 2n+1, \cdots, (m-1)n+1 \quad (12)$$

in which h_{in} and h_{out} are the pressure head of flow at the inlet boundary and the outlet boundary, respectively.

The pressure head of flow at each cell remains to be an unknown variable if the aperture width distribution of a fracture is known. Most of studies

for the variable aperture model have applied the aperture width distribution obtained by a random number generator in computer [11-14], however, the method cannot define the value of aperture width for a specific position and predict the migration profile in time and space in a fracture.

2.2. Tracer Transport

In the variable aperture channel model, the tracer transport through a fracture can be calculated by a particle-tracking technique [16] provided that the distribution of flow rates in a fracture is given. The flow rate through each cell is obtained using Eqs.(3) through (12).

In the particle tracking method, the calculation of residence time of particles in individual cell is essential to obtain the elution profile of a tracer. The residence time of particles in each cell depends on the mass transport phenomena that they take part in. Since all particles move in fracture randomly, the normalized mass flux equation can be used as a probability density function to give the residence time of particle in a cell. The normalized mass flux equation for particles introduced into a cell with step injection can be classified into the following three cases.

Case I : considering only convective flow in cell

$$C_f' = U(t - t_{w,i}) \tag{13}$$

Case II : considering convective flow and surface sorption in cell

$$C_f' = U(t - t_{o,i}) \tag{14}$$

Case III : considering convective flow and surface sorption in cell as well as diffusion into rock matrix

$$C_f' = erfc\left(\frac{t_{o,i}}{2\alpha\sqrt{t_{sd,i} - t_{o,i}}}\right) \tag{15}$$

where

$$t_{w,i} = \frac{\bar{b}_i \Delta x \Delta z}{\frac{1}{2}(q_{i,1} + q_{i,2} + q_{i,3} + q_{i,4})} \tag{16}$$

$$t_{o,i} = R_{a,i} t_{w,i} \tag{17}$$

$$R_{a,i} = 1 + \frac{2}{\bar{b}_i} K_a \tag{18}$$

$$\alpha_i = \frac{R_{a,i}\bar{b}_i}{2\phi\sqrt{D_p R_d}} \tag{19}$$

The function $U(t)$ is the step function with unity for $t > 0$. The terms $t_{w,i}$ and $t_{o,i}$ are the water residence time and the residence time of particle delayed by surface sorption within cell i, respectively. The lumped parameter α_i represents the relative contribution of rock matrix diffusion to the surface sorption.

The residence time of a particle for each case is calculated by the inverse function of Eq.(13), (14) and (15), respectively. The residence time of particle in cell i for cases I and II is given to $t_{w,i}$ and $t_{o,i}$, respectively, regardless of the value of particle density (C_f'). For case III, the residence time of particle in cell i, $t_{sd,i}$, is a function of particle density value expressed by

$$t_{sd,i} = t_{o,i} + \left(\frac{a t_{o,i}}{2\alpha_i}\right)^2 \tag{20}$$

where

$$a = 1/erfc^{-1}(r_N) \tag{21}$$

The term r_N is a random number to represent the value of normalized particle density between 0 and 1. The random number should be generated from uniform distribution because all physicochemical processes in fractures are with the same

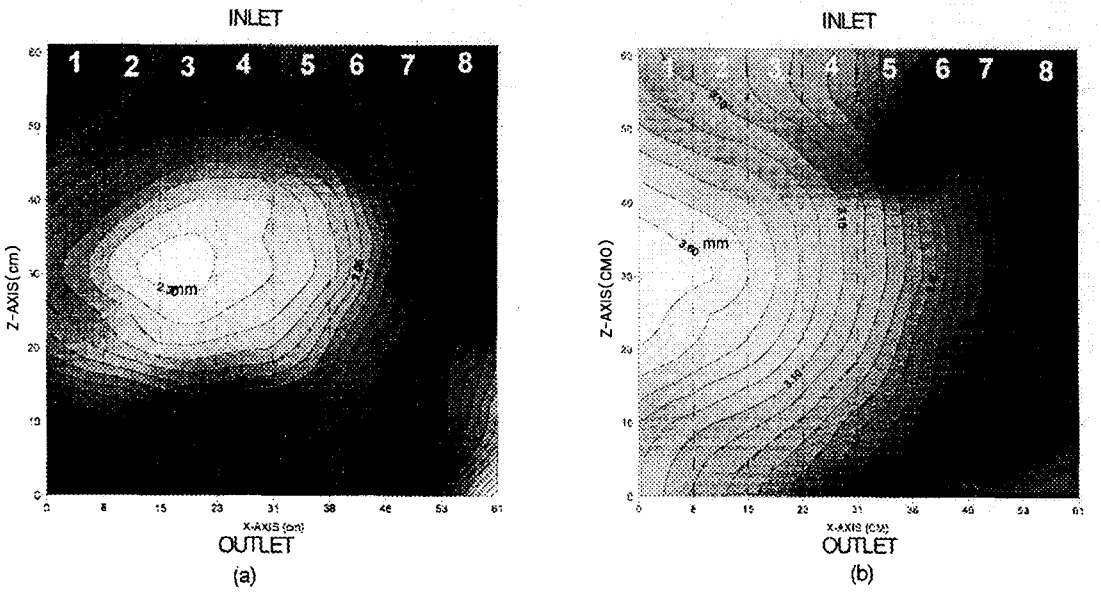

Fig. 3. Aperture Width Distributions for (a) the Parallel and (b) the Wedge-Shaped Fracture.

probability of occurrence. Actually, Eq.(20) is a generalized equation including cases I and II. The term $t_{sd,i}$ reduces to $t_{o,i}$ when rock-matrix diffusion is insignificant ($\alpha \rightarrow \infty$) and is identical to $t_{w,i}$ when both sorption and rock-matrix diffusion are insignificant.

Finally, we can obtain the total residence time of a particle by summing all the residence times traversed by the particle over the entire path from inlet to outlet :

$$t_R = \sum_{i=1}^{N_e} t_{sd,i} \tag{22}$$

where N_e is the number of cells that particle has passed through.

3. Experiment

3.1. Artificial Fracture Generation

The parallel fracture was made by assembling a slab of polished pink granite (10.16 × 61 × 61 cm) and a transparent acrylic plastic sheet (10.1 × 61 × 61 cm). The spacers that were fabricated from stripes of stainless steel of 0.158 cm thick were placed at both ends of the fracture, parallel to the direction of flow. The pink granite slab was painted white to ease the observation of the plume of conservative tracer as it moved through the fracture. After the migration experiments in the parallel fracture had been completed, the spacer of one side was replaced by a spacer of 0.316 cm thick to form a wedge-shaped fracture.

Because the granite slab was not perfectly flat, before assembling, the distance between the granite surface and a perfect flat surface were measured using a calibrated straight edge and feeler gauges at irregular grid points. The measured values were converted into regularly spaced data using a commercially available program (SURFER) and added to the spacer thickness to obtain the actual aperture width distribution between the two slabs. The

Table 1. Input Parameter Values Used in the Calculation.

- acceleration due to gravity (g) = 980 cm/s^2
- density of water (ρ) = 1.0 cm^3/g
- dynamic viscosity of water (μ) = 1.124 cP =1.124 × 10^{-2} g/cm.s
- total flow rate (Q) = 30 mL/hr
- fracture length (L_z) = 61 cm
- fracture width (L_x) = 61 cm
- average aperture width ($\overline{b}$) = 0.193 cm for the parallel fracture
  = 0.272 cm for the wedge-shaped fracture
- convergent criterion = 10^{-10}
- numbers of cells ($m \times n$) = 32 × 32

calculated fracture volume was about 718 mL for the parallel fracture and 1012 mL for the wedge-shaped fracture. Fig.3 (a) and (b) shows contour maps of the aperture width distribution for the parallel and the wedge-shaped fracture, respectively. The map shows a larger aperture width in the middle zone in the parallel fracture due to the concavity produced during the polishing of the granite surface. For the wedge-shaped fracture the aperture width decreases monotonously along the transverse direction (x-axis) and the concavity effect is not evident.

3.2. Migration Experiments

For migration experiments acrylic inlet and outlet reservoirs were attached to two sides of the artificial fracture. Porous polyethylene membranes with uniform pore size of 40 micrometers were inserted to decrease the dead volume between the inlet reservoir and the fracture. The outlet reservoir was divided into eight equal sections to enable the flow from each different area of the fracture to be collected with individual fractional collector. Distilled and deionized water (DDW) was pumped through the fracture at a flow rate of 30 mL/hr (Q_T). A 2 × 10^{-4} mole/l (C_{in}) uranine (Fluorescein sodium salt, $C_{20}H_{10}Na_2O_5$) was used as the conservative dye. The dye injection was ceased after 24 hours (t_{in}) and the fracture flushed with water. These migration experiments were done over periods of 48 hours. The movement of uranine front was photographed with every 3 hours intervals.

4. Results and Discussion

4.1. Flow Distributions

The input parameter values for calculations of flow distribution lists at Table 1. The fracture was divided into 32 × 32 cells, total 1,024 cells. The pressure head at the fracture inlet (h_{in}) was calculated using Eq.(1) and the pressure head at the fracture outlet (h_{out}) was assumed to be unity. The linear algebra equations resulted from Eq.(3) through Eq.(12) were solved by the Gauss-Seidel iteration method [17] with the convergent criterion of 10^{-10}.

Fig.4 (a) and (b) shows the calculated transverse and the longitudinal flow rate in the parallel and the wedge-shaped fracture, respectively. The length of arrows shown in the figure is proportional to the magnitude of the

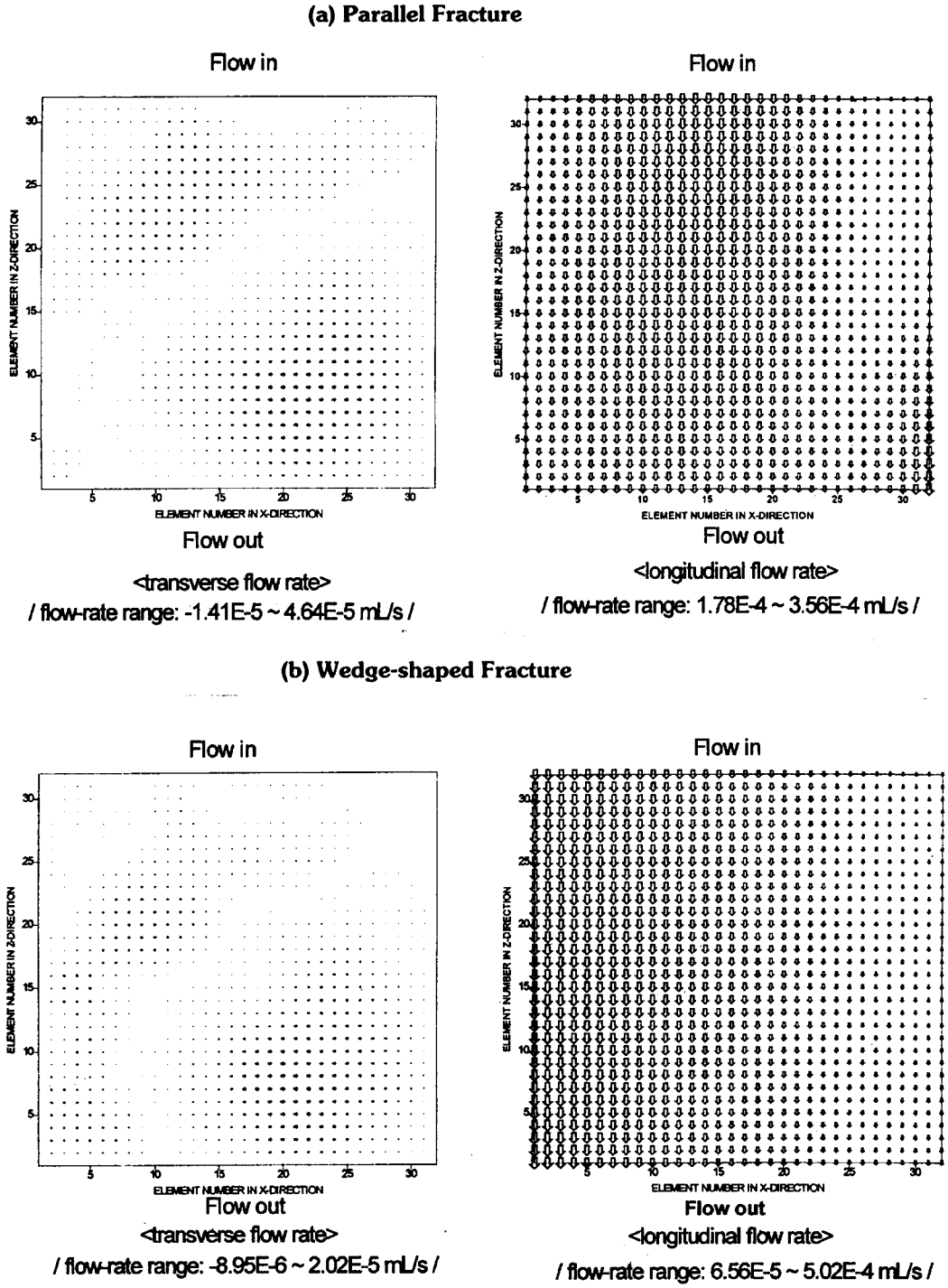

Fig. 4. Distribution of Transverse (q_3) and Longitudinal Flow Rate (q_1) in the (a) Parallel and (b) the Wedge-Shaped Fracture Calculated by the Variable Aperture Channel Flow Model.

flow rate. For the parallel fracture the longitudinal flow rate is the largest in the middle zone of the fracture due to the concavity of the fracture. The transverse flow rate is about factors of ten less than the longitudinal flow rate. It can be predicted that the force acting normally to the flow direction is unlikely to affect the overall flow pattern. All longitudinal flow rates are within same orders of magnitude although the flow rate is inversely proportional to the third power of aperture width. It suggests that the aperture width of the fracture designed for this experiment is not so various. For the wedge-shaped fracture the longitudinal flow increases with the aperture width. Similarly with the parallel fracture case, the transverse flow rate is negligible compared with the longitudinal flow rate, indicating a minor effect of transverse flow.

4.2. Migration of Uranine

Migration of uranine was predicted by tracking the particles advected through fractures. In this work, physicochemical parameters α and R_a could be neglected because the rock matrix diffusion and sorption can be ignored in the granite surface coated with epoxy paint.

Calculations have been performed with about 20,000 particles, sufficiently large number to avoid spurious results. Before calculating elution profile, we counted numbers of particles entering cells in contact with the inlet boundary and exiting cells in contact with the outlet boundary to check if random number was adequate to determine the pathway of each particle. Figs.5 and 6 are bar graphs of numbers of particles at the inlet and outlet of the parallel and the wedge-shaped fracture, respectively. For both fractures the particle distribution was well corresponded to the aperture width at the inlet and outlet of each fracture shown in Fig.3 and the number of particles were proportional to the flow rate (third power of the aperture width) of a given cell. It proved that the random number was uniformly well generated and the probability toward a specific outflow direction within a cell was well proportional to the outflow rate.

Fig.7 shows the elution profile of uranine at eight individual outlet ports of the parallel and the wedge-shaped fracture, respectively. The vertical axis in the figures gives the relative concentration, the ratio of accumulated numbers of particles, which have arrived at each port up to a time t to total accumulated numbers. For the parallel fracture elution profiles for ports 3 and 4 had the earliest breakthrough time, suggesting the concavity effect of fracture, while for the wedge-shaped fracture the concavity effect was not observed. Since breakthrough time increases with the decrease of aperture width, the breakthrough curves show to be delayed in the narrower aperture width zone in both fractures. The elution order of breakthrough curves may be quantitatively predicted by the water retention time provided that channels in fractures are independent of each other. Table 2 shows the mean retention time of water through each channel in fracture calculated by cubic' s law. The retention time of curves is increased in port 4-3-5-2-1-6-8-7 sequence for the parallel fracture and port 1-2-3-4-5-6-7-8 sequence for the wedge-shaped fracture. These results are well agreed with the elution sequence of most breakthrough curves in Fig.7. However, in Fig.7(a) the curve for the port 6 elutes earlier than that for the port 1 although the average retention time are very similar for both ports 1 and 6. This earlier elution for the port 6 is

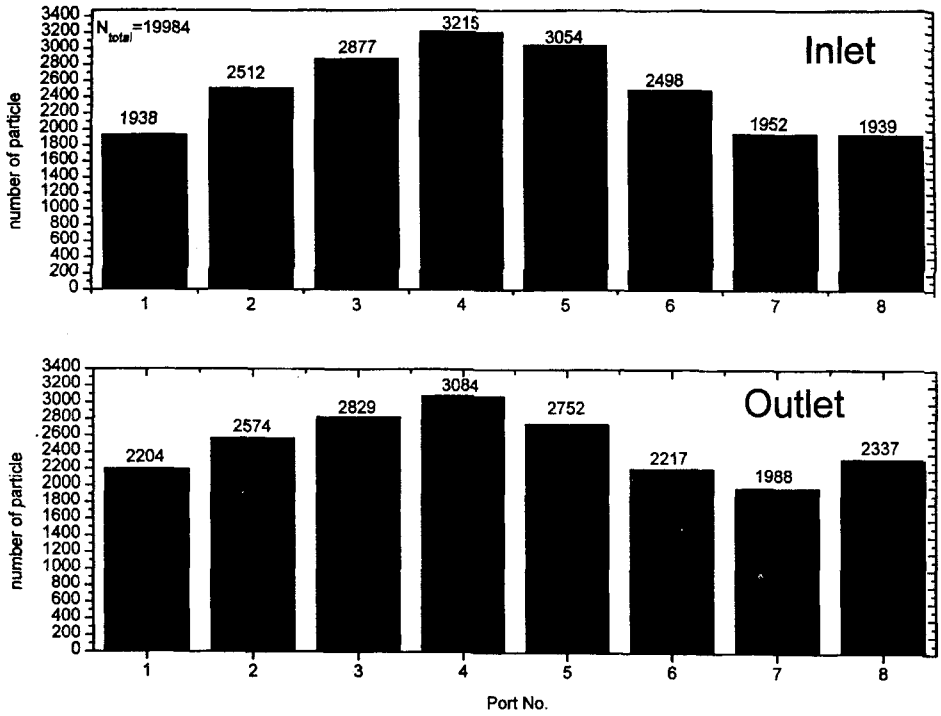

Fig. 5. Particle Distribution at Inlet and Outlet of the Parallel Fracture.

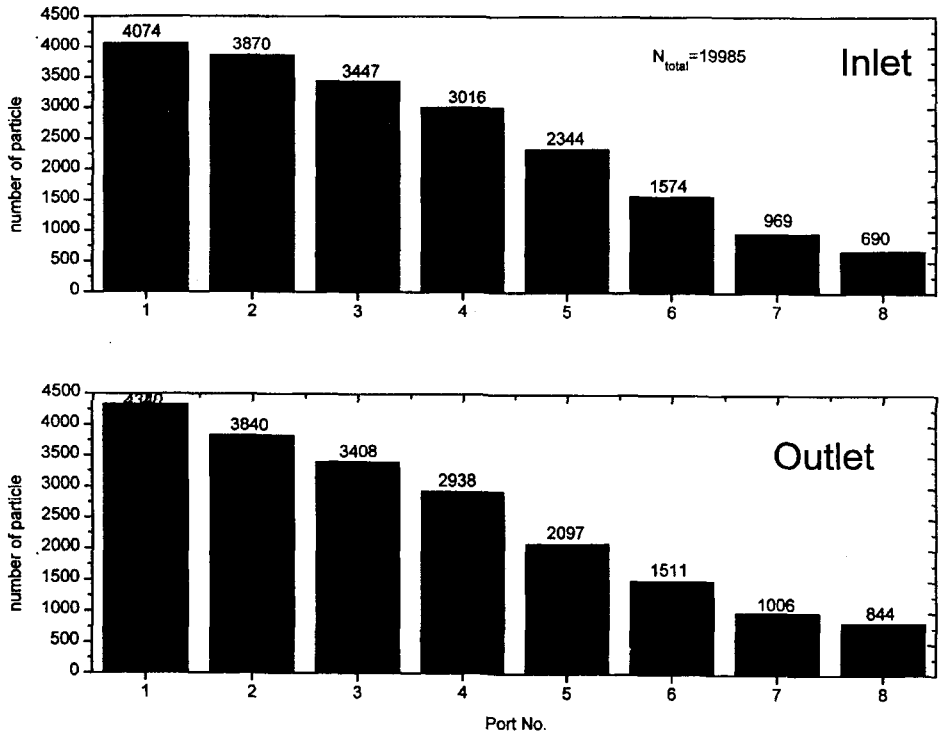

Fig. 6. Particle Distribution at Inlet and Outlet of the Wedge-Shaped Fracture.

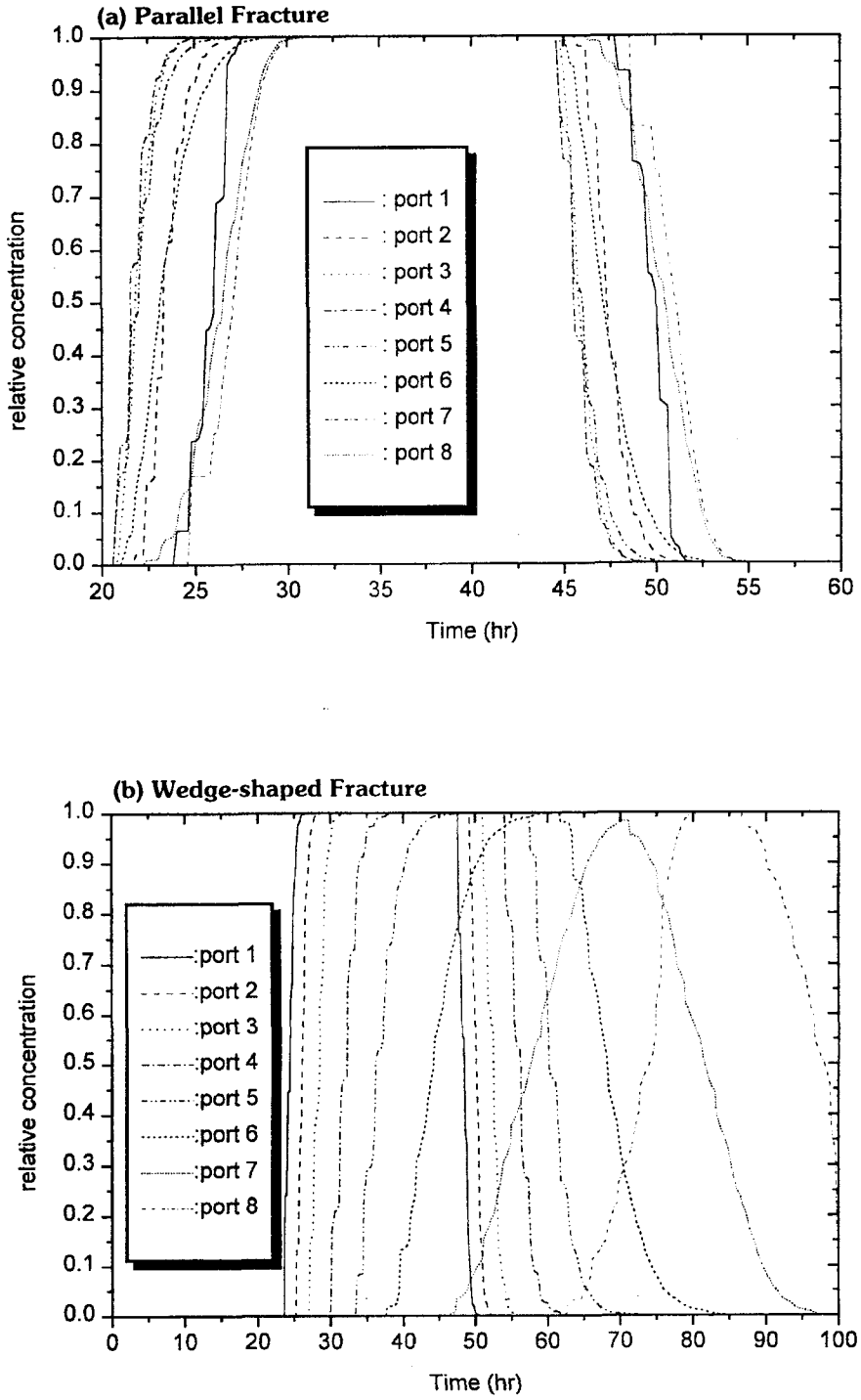

Fig. 7. Elution Profiles of Uranine for the Eight Individual Outlet Ports Obtained in the (a) Parallel Fracture and (b) the Wedge-Shaped Fracture.

likely to be caused by intermixing between adjacent channels. We can see from Fig.3(a) that the transverse flow rates in the area corresponding to channels 3 to 6 (larger aperture width and higher water flow rates zone) are relatively greater than those in the edge zone of the parallel fracture (channels 1, 2, 7, 8). This fact indicates that the intermixing between channels, although its effect on overall flow pattern is small, would occur in the center zone of the parallel fracture. This intermixing will make the fraction of particles introduced into the channel 6 move through the adjacent channel 5 with higher flow rates and conclusively result in shorter retention time of particles for the channel 6. This is why the curve for the port 6 elutes earlier than that for the port 1.

We are interested not only in the breakthrough time but also in the channel dispersion. The slope of leading zone of elution curve can account for the extent of channel dispersion. The steep rising in the concentration curve corresponds to small channel dispersion. We can see that the leading edge of most elution curves for in the parallel fracture is hardly dispersed. This implies the existence of small channel dispersion. Since the channel dispersion is caused by the aperture width distribution, giving the difference in velocity between channels, if we refer to the standard deviation of aperture width in Table 2, the reason of such a small channel dispersion becomes clearer. The values of standard deviation of aperture width for all channels are less than 10% of its mean value. This distribution of aperture width is not likely to cause evident channel dispersion. On the other hand, the elution curves for ports 6 through 8 in the wedge-shaped fracture are apparently more dispersive than other curves. This result does not mean larger channel dispersion in those channels. Table 2 shows that the standard deviations for channels 6 and 7 in the wedge-shaped fracture are smaller that those for other channels, which mean rather smaller channel dispersion. Accordingly, the relatively larger dispersivity of curves for ports 6 through 8 in the wedge-shaped fracture is likely to be caused by not the channel dispersion but the long retention times due to low flow rates.

On the other hand, the stair-step structure, although it is not so large, is shown in a number of elution curves. This is due to the finite delay for the tracer and is a typical evidence of channel dispersion. The earlier arrivals of tracer correspond to flow in faster channels with a very small aperture constrictions and later arrivals to flow in slower channels. This stair-step shape of curve cannot be predicted by one-dimensional model such as the hydrodynamic dispersion diffusion model in which a uniform flow rate is assumed [1,3].

Figs.8 and 9 show the comparison between the calculated and photographed migration plumes of uranine for the parallel and the wedge-shaped fracture, respectively. For the parallel fracture, the flow through the center zone with greater aperture width is faster than that at the edges with smaller one. Six hours after the start of the uranine injection, the leading edge of the dye had moved approximately 13 cm along the edges of the parallel fracture, while the center of the front had moved 17 cm. This corresponds to the mean moving velocity of about 2.5 cm/hr to give mean residence time for about 24 hours in the parallel fracture. As expected, the photographed result shows evidently the concavity effect in the middle zone in the parallel fracture and agrees well with the geometric shape of fractures. For the parallel fracture, good agreement was found between

Table 2. Mean Aperture Width ($\bar{b}_i$), Standard Deviation (σ), Mean Flow Rate (Q_i) and Water Retention Time (t_w) for Each Channel in Fracture.

	Parallel fracture				Wedge-shaped fracture			
Channel	$\bar{b}_i$ (cm)	$\sigma/\bar{b}_i$(cm) (%)	Q_i (mL/hr)	t_w(hr)	$\bar{b}_i$(cm) (cm)	$\sigma/\bar{b}_i$(cm) (%)	Q_i (mL/hr)	t_w(hr)
1	0.190	10.53	3.51	25.16	0.338	5.96	6.46	24.32
2	0.199	10.65	4.05	22.84	0.327	6.49	5.67	25.93
3	0.205	10.10	4.44	21.49	0.314	6.77	5.19	28.18
4	0.205	9.05	4.45	21.46	0.294	6.69	4.26	32.11
5	0.201	8.20	4.19	22.35	0.271	6.76	3.32	37.95
6	0.189	6.30	3.47	25.32	0.238	6.31	2.27	48.91
7	0.177	4.20	2.83	29.01	0.206	4.99	1.47.	65.18
8	0.181	7.80	3.05	27.60	0.191	7.03	1.16	76.30

the calculated and the observed front. For the wedge-shaped fracture the fracture geometry dominates the flow pattern and the predicted concentration front in the center zone seems to represent the experimental data roughly well even though the effect of the concavity is not shown in the calculated result. However, in the photographed plume for the wedge-shaped fracture, the stagnant zone of water appears in the edge zone with the smallest aperture width, while the model can not predict such a water stagnant zone. This water stagnant zone seems to be produced due to an additional force enough to prevent the convective flow of water through the zone. Although the exact reason has not been known, the flow resistance force such as surface tension can be a major cause producing such a water stagnant zone. In this water stagnant zone the diffusion will be more dominant process than convective flow. However, modeling such a wall effect that produces the water stagnant zone may be very difficult because the exact boundary between the convective flow zone and the stagnant water zone cannot be defined. In addition, considering that such a wall effect in the wedge-shaped fracture can be a minor problem when the width of fracture is very large like actual natural fractures, such a wall effect may be not so critical. In spite of difference between model and experiment for edge zone in the wedge-shaped fracture, the comparison result between the calculated and the photographed plume for both fractures give us confidence that the present model can be effective to predict heterogeneous flow field.

5. Conclusions

In order to validate the variable aperture channel model, migration experiments of conservative tracer were performed in two artificial fractures, a parallel and a wedge-shaped fracture. The migration plumes of uranine as conservative tracer were photographed to obtain profile in space and time in the fracture. The results are summarized as follows.

1) The transverse flow rates in both fractures were negligible, compared to the longitudinal flow rate. This suggested that the transverse flow would be an insignificant factor to the overall flow pattern.

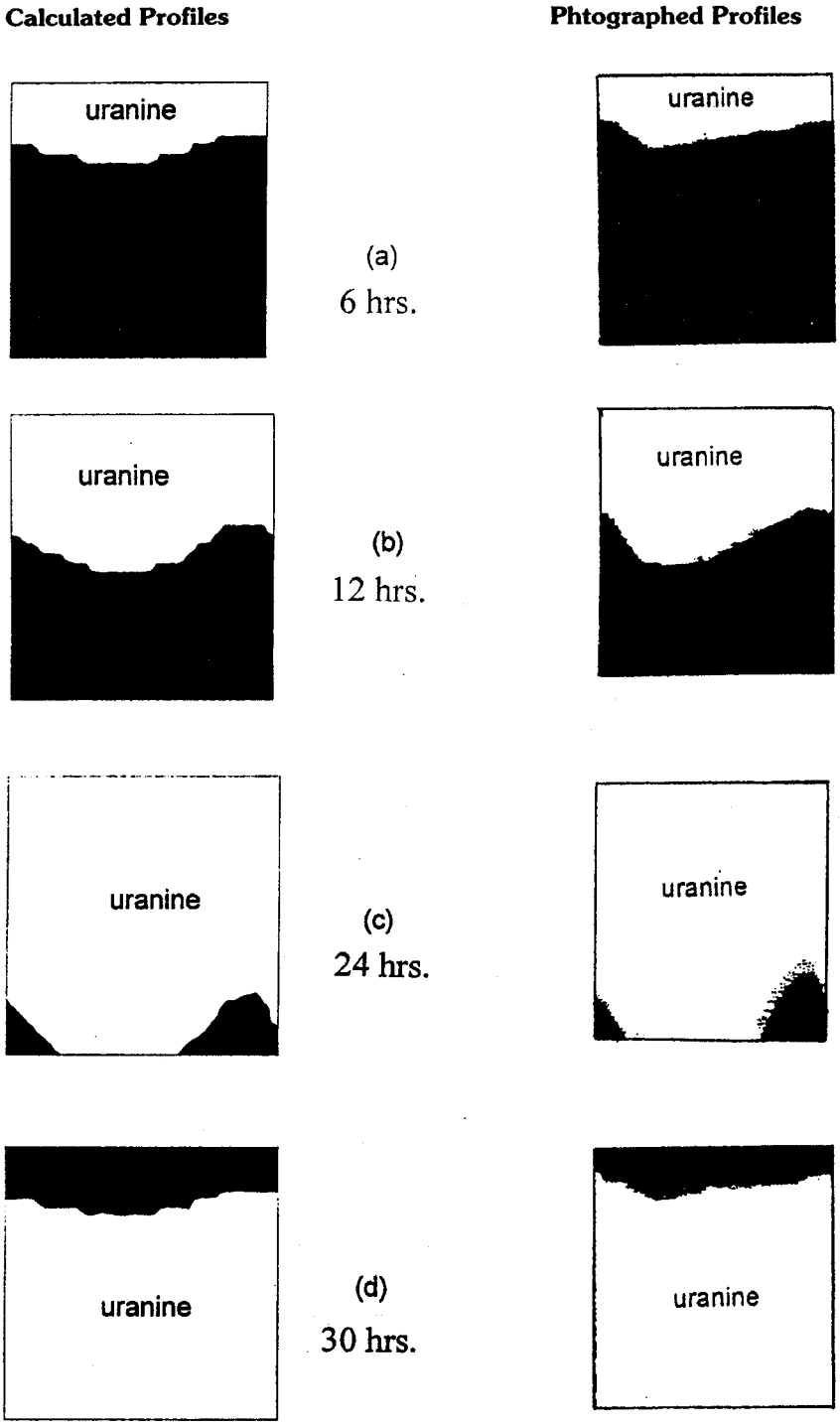

Fig. 8. Comparison Between Calculated and Photographed Migration Plume of Uranine After (a) 6, (b) 12, (c) 24 and (d) 30 Hours Obtained in the Parallel Fracture.

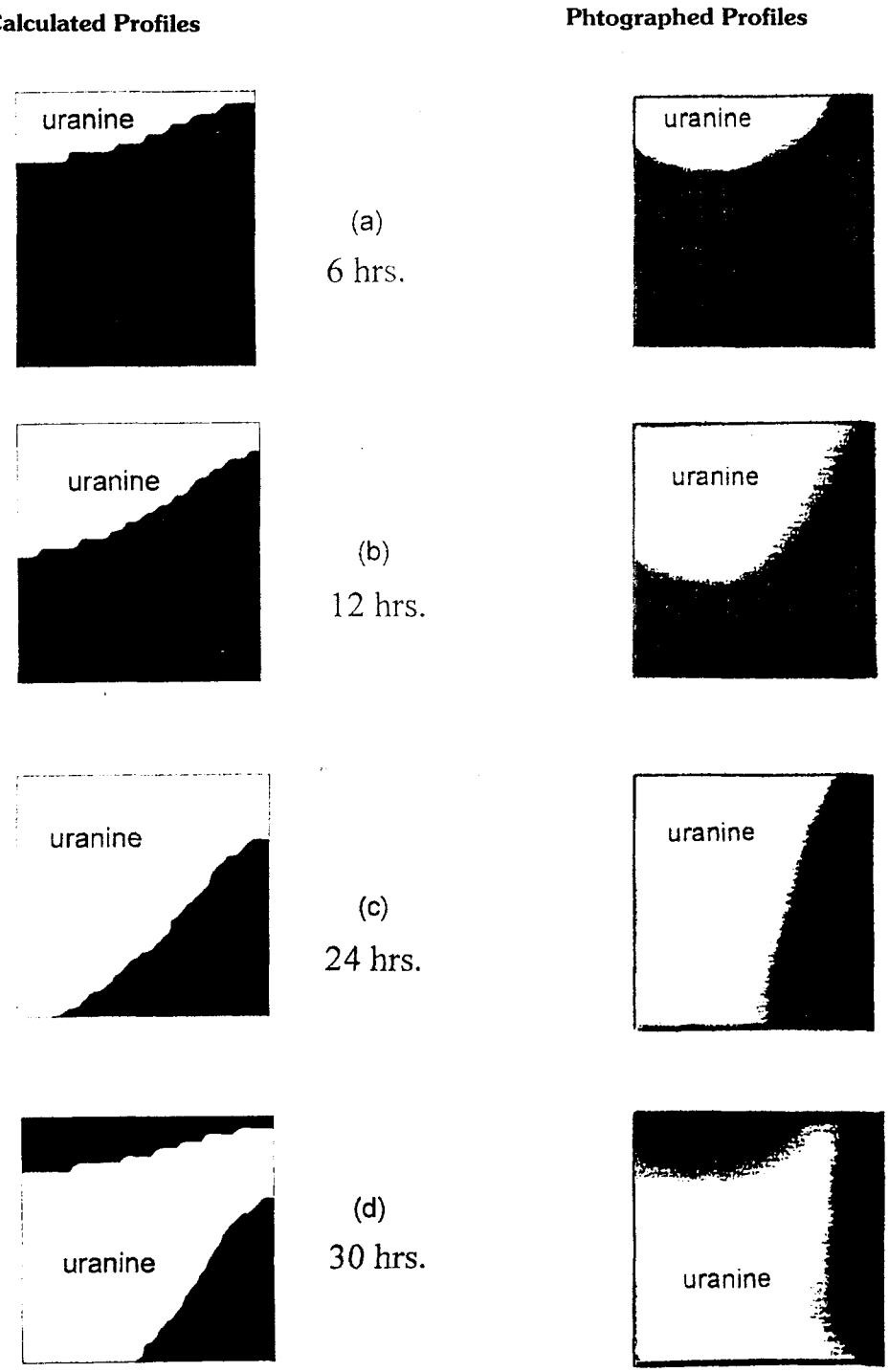

Fig. 9. Comparison Between Calculated and Photographed Migration Plume of Uranine After (a) 6, (b) 12, (c) 24 and (d) 30 Hours Obtained in the Wedge-Shaped Fracture.

2) The channel dispersion for each channel was small because the variation of aperture width was not so significant.
3) The variable aperture channel model showed the stair-step structured elution curve, a typical evidence of channel dispersion.
4) A good agreement was found between the photographed migration plume and those predicted by the variable aperture channel mode, especially for the parallel fracture.

Conclusively, migration experiment to validate transport model should be addressed to produce data that can be compared directly with the model. Therefore, the direct observation of migration plume of tracer attempted in this study must be very interesting approach. The results of this study give us the confidence that the variable aperture channel model would be effective to deal with heterogeneous flow field.

References

1. Tang, D.H., E.O. Frind and E.A. Sudicky, "Contaminant transport in fractured porous media: An analytical solution for a single fracture, Water Resour. Res., vol 17, p555, (1981).
2. Neretnieks, I., T. Eriksen and P. Tahtinen, "Tracer movement in a single fissure in granite rock : Some experimental results and their Interpretation", Water Resour. Res., vol 18, p849,(1982).
3. Moreno, L. I Neretnieks and T. Eriksen, "Analysis of some laboratory tracer runs in natural fissures", Water Resour. Res., vol 21, p951, (1985).
4. Fujikawa, Y., M. FuKui, D.J. Drew and T.T. Vandergraaf, "Analysis of the migration of instantaneously injected cesium in artificial fractures of Lac du Bonnet granite,Manitoba Canada", J. of Contam. Hydro., vol 14, p207, (1993).
5. Keum, D.K., W.J. Cho, P.S. Hahn and H.H. Park, "Study on radionuclide migration modeling for a single fracture in geological medium", J. Korean Nuclear Soc., vol 26, p402, (1994).
6. Gustafsson, E. and C.E. Klockars, "Study of strontium and cesium migration in fractured crystalline rock", KBS Technical Report 84-07, (1984).
7. Birgersson, L., H. Widen and T. Argen, "Tracer experiments in the Stripa mine 1980 ~1991", SKB Technical Report 92-25, (1992).
8. Hadermann, J. and W. Heer, "The Grimsel (Switzerland) migration experiment : integrating fields experiments, laboratory investigations and modeling", J. of Contam. Hydro., vol 21, p87, (1996).
9. Neretnieks, L., "A note on fracture flow dispersion mechanism in the ground", Water Resour. Res., vol 19, p364, (1983).
10. Keum, D.K., C.K. Park, P.S. Hahn and T.T. Vandergraaf, "A stratified channel model with local longitudinal dispersion", Nuclear Technology, December vol 120, p211, (1997).
11. Tsang, Y.W. and C.F. Tsnag, "Channel model of flow through fractured media", Water Resour. Res., vol 23, p467, (1987).
12. Tsang, Y.W. , C.F. Tsang, I. Neretnieks and L. Moreno, "Flow and tracer transport in fractured media : A variable aperture channel model and its properties", Water Resour. Res., vol 24, p2049, (1988).
13. Moreno, L., Y.W. Tsang, C.F. Tsang, F.V. Hale and I. Neretnieks, "Flow and tracer in a single fracture: A stochastic model and its relation to some field observations", Water Resour. Res., vol 24, p2033, (1988)
14. Kimura, H. and M. Munakata, "Analysis of

tracer movement in single fracture in granite core (INTRAVAL: case 2)", J. Nuclear Sci. &Tech., vol 28, p1115, (1991).

15. Park, C.K., P.S. Hahn and T.T. Vandergraaf, "Analysis of the migration of nonsorbing tracers in a natural fracture in granite using a variable aperture channel model", *J. of Contam. Hydro.* vol 26, p97, (1997)
16. Robin, P.C., Connectivity, flow and transport in network models of fractured media, Ph.D. Thesis, St. Catherine's, Oxford University, Ref. TP1072, p118, (1984).
17. Carnahan, B., H.A. Luther and J. O. Wilks, Applied Numerical Methods, John Wiley & Sons, Inc., p100, (1969).